energies

MDPI

Article

A Method for Optimal Allocation of Distribution Network Resources Considering Power–Communication Network Coupling

Kaitao Sun [1], Jiancun Liu [1,*], Chao Qin [2,*] and Xi Chen [1]

[1] School of Electrical Engineering and Automation, Tianjin University of Technology, Tianjin 300384, China; sunkaitao@stud.tiut.edu.cn (K.S.); chenxi1@stud.tiut.edu.cn (X.C.)
[2] School of Electrical and Information Engineering, Tianjin University, Tianjin 300072, China
* Correspondence: liujiancun@email.tjut.edu.cn (J.L.); qinchao@tju.edu.cn (C.Q.)

Abstract: With the development of distribution networks, the widespread use of communication devices has exposed these networks to the risk of cross-domain attacks. Based on the coupling relationship between power and communication networks, a method for the optimal allocation of distribution network resources considering this coupling is proposed. In the resource allocation stage, given the limited availability of resources, optimal allocation is carried out for resources such as distributed generations and remote-controlled switches; additionally, the resilience of the distribution network is enhanced through the reinforcement of both the distribution lines and communication links. In the prevention stage, in advance of extreme events, preventive islanding is formed through switch operations. In the degradation stage, the distribution network identifies faulted and non-faulted areas based on the fault propagation model, while the communication network assesses the fault status of communication nodes based on the virtual flow model. In the recovery stage, coordinated control of remote-controlled switches and distributed generations with normal communication is implemented for network reconfiguration to minimize load losses. Finally, the effectiveness of the proposed method is verified through the IEEE 33-node system.

Keywords: distribution network; communication network; resilience; distributed generation; remote-controlled switch; network reconfiguration

check for updates

Academic Editor: Santi Agatino Rizzo

Received: 2 January 2025
Revised: 23 January 2025
Accepted: 27 January 2025
Published: 30 January 2025

Citation: Sun, K.; Liu, J.; Qin, C.; Chen, X. A Method for Optimal Allocation of Distribution Network Resources Considering Power–Communication Network Coupling. *Energies* **2025**, *18*, 644. https://doi.org/10.3390/en18030644

Copyright: © 2025 by the authors. Licensee MDPI, Basel, Switzerland. This article is an open access article distributed under the terms and conditions of the Creative Commons Attribution (CC BY) license (https://creativecommons.org/licenses/by/4.0/).

1. Introduction

With the intellectualization of distribution systems, traditional distribution networks have integrated communication and sensing technologies to form a cyber–physical system (CPS) [1]. Advanced communication technologies provide robust support for the operation of distribution networks. However, during extreme events, the coupled relationship between the power and communication networks may exacerbate the vulnerability of the distribution network, potentially leading to large-scale blackouts [2]. For example, in 2015, Ukraine experienced a cyber-attack that resulted in widespread power outages in multiple regions [3]. Based on the fault-handling process during extreme events, the state of the distribution system facing the extreme events can be divided into four stages: resource optimization and allocation, prevention, degradation, and recovery [4]. Therefore, under the complex conditions of multi-stage correlation in extreme events and the coupling of multiple network systems, how to effectively coordinate and utilize flexible resources at

both the information and physical levels to mitigate the impact of extreme events on the distribution network is an urgent problem that needs to be addressed [5].

There has been extensive research on methods to enhance the resilience of distribution networks under extreme events from the power network aspect itself. Reference [6] developed a distribution network planning model that incorporates situational awareness. Reference [7] explored risk-based long-term planning for distribution networks, aiming to improve resilience against extreme events through investments in reinforced lines and smart grid technologies. Reference [8] proposed a cooperative optimization scheme for anti-icing and de-icing in distribution networks, integrating intelligent soft-switching technology and an energy storage system. Reference [9] established a post-disaster recovery strategy for distribution networks, considering the impact of changes in traffic volume on mobile energy storage scheduling within coupled transportation–electricity networks. Reference [10] constructed an efficient active defense scheduling strategy, utilizing a rolling optimization approach to enhance the defense capability of distribution networks. Reference [11] effectively coordinated and utilized multiple resources, such as distributed generations (DGs), fault indicators (FIs), and manual switches (MSs), to optimize the resilience of distribution networks against extreme events.

On the other hand, research on resilience enhancement methods from the communication network aspect has also been conducted. For instance, reference [12] proposed a post-disaster restoration scheme for distribution networks that combines wired and 5G wireless communication networks. Reference [13] introduced a robust optimization method for communication networks under extreme events, based on information flow and communication-network-associated load ability indicators. However, these studies primarily focused on single power systems or communication systems and did not consider the impact of multi-system coupling relationships on distribution network resilience. In reference [14], a scheme for remote-control switch (RCS) configuration and communication enhancement under the coupling constraint of a power–communication network is established, and in the case of a cyber–physical coordinated attack, the RCS configuration is optimized. Reference [15] utilized emergency communication vehicles to rapidly set up a wireless communication network after a disaster, coordinating the dispatching of maintenance personnel and switch operations to improve the resilience of the distribution system. Reference [16] proposes a resilience assessment framework for cyber–physical power systems (CPPS), which considers the spatiotemporal indexes of disasters and the interaction between information systems and power grids, including fault scenario extraction, response and recovery analysis, and quantitative resilience assessment, focusing on building a resilience assessment framework. References [17,18] proposed a distribution network restoration strategy combined with communication, utilizing unmanned aerial vehicles (UAVs) for wireless communication restoration. Although these studies considered the coupling between multiple networks, the interconnections between different stages after an extreme event or the optimal allocation of multiple resources in the pre-event allocation stage are not fully addressed.

Therefore, this paper proposes a method for the optimal allocation of distribution network resources considering the coupling between power and communication networks. The coupling relationship between the communication network and the distribution system is analyzed. Based on this, the fault-handling process under extreme events is considered. In the resource allocation stage, various resources such as DGs and RCSs are optimally allocated. Additionally, the resilience of the distribution network is enhanced through reinforcement of both the distribution lines and communication links. In the prevention stage, network reconfiguration is conducted in advance to form preventive islands. In the degradation stage, faulted and non-faulted areas are identified based on the fault

propagation model, and the fault status of communication nodes is determined using the virtual flow model. In the recovery stage, considering the coupling relationship between multiple network systems, RCSs with normal communication are utilized for fault isolation and coordinated with DGs to form restorative islands. Through the optimal allocation of resources and their collaboration across multiple stages, the resilience of the power–communication coupled distribution network can be jointly enhanced.

2. Problem Statement

The coupling relationship between the distribution network and communication network is illustrated in Figure 1. The communication network is responsible for transmitting information and monitoring the state of the distribution network, while the distribution network controls the operational state and ensures the effective implementation of strategies. During normal operation, the distribution network also provides a stable energy supply to the communication nodes within the communication network. Therefore, the power network and communication network functionally complement each other, providing a robust guarantee for the safe and stable operation of the distribution network.

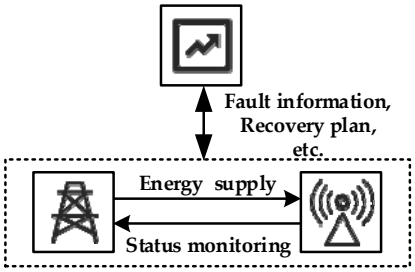


Figure 1. Coupling relationship between the distribution network and communication network.

In a typical fault scenario, the distribution system usually experiences a single electrical fault. At this point, the fault propagates through the closed lines. After locating the fault, the operational center can use the RCS to cut off the fault propagation path, forming a faulted area and a non-faulted area. Then, through network reconfiguration, the load can be transferred to restore the system from the fault.

In the event of extreme conditions, both the distribution network and communication network may simultaneously malfunction, causing damage to the overall system. The failure of the communication network hinders the operational center's ability to swiftly obtain real-time information about the affected area. Consequently, traditional distribution system restoration methods become ineffective, potentially rendering load restoration impossible after extreme events. To this end, it is necessary to optimize the allocation of various resources to ensure the effective transmission of fault information, a recovery plan, etc., in the communication network, thereby enhancing the resilience of the distribution network against extreme events.

The resilience of multi-network systems focuses more on the coupling between multiple stages before and after extreme events as opposed to single-network systems. For instance, if certain lines fail in the power network, the subsequent degradation and recovery stages will lead to loss of load, which may influence network reconfiguration decisions during the prevention stage in turn. Furthermore, the correlation between these stages also encompasses the coupling relationship between the power network and communication network. For example, a power outage in a specific area may disrupt communication services, and vice versa, a communication failure can prevent the power network from effectively managing and rerouting power flows. This interaction significantly affects re-

silience enhancement strategies. Therefore, enhancing resilience in a multi-network system necessitates a holistic consideration of the interactions among various stages and networks.

3. Model Formulation

In this section, considering the coupling relationship of the distribution network and the communication network, the optimal model of RCS and DG allocation, as well as distribution line and communication link reinforcement, is established, the model framework of which is shown in Figure 2. The uncertainty of communication network fault and distribution network fault is considered in a scenario-based stochastic optimization model.

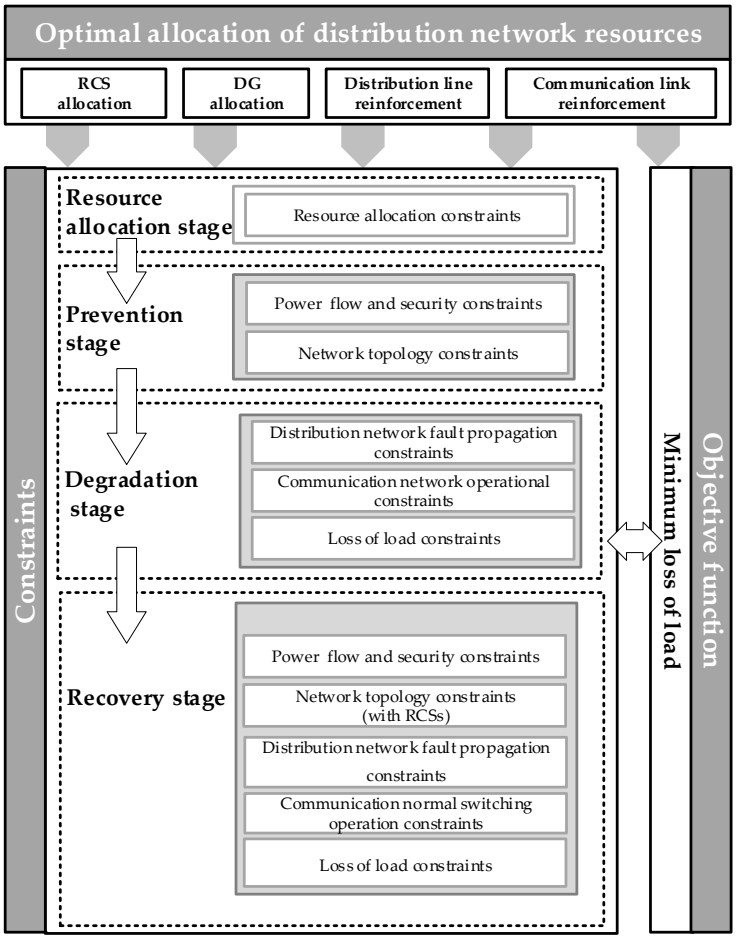


Figure 2. Framework of the proposed model.

3.1. Resource Allocation Constraints

In the context of the distribution network, to address potential fault risks, specific reinforcement measures are taken for the distribution lines to enhance their resilience against impending extreme conditions. Additionally, RCSs and DGs are deployed to enable rapid isolation and restoration in case of faults, while relying on the DG to form islands, thereby achieving rapid power restoration. In the context of the communication network, strategies are adopted to reinforce communication links, ensuring the communication links remain functional even under attacks.

Based on economic and feasibility considerations, too many RCSs and DGs increase costs, and when the number of RCS reaches a certain threshold, the growth rate of the system load percentage might begin to slow down. For this purpose, the maximum number of RCSs and DGs is defined, as shown in Equations (1) and (2). Reinforcing all lines and communication links across the board would impose a huge economic burden and would

not be practical. Therefore, it is necessary to set a reasonable ceiling on the number of reinforcements to ensure cost effectiveness, as shown in Equations (3) and (4).

$$\sum_{\forall i \in \Omega_l^{\text{bus}}} s_{i,l}^{\text{rcs}} \le N^{\text{rcs}}, \forall l \in \Omega^{\text{line}} \tag{1}$$

$$\sum_{\forall i \in \Omega^{\text{bus}}} m_i^{\text{dg}} \le N^{\text{dg}} \tag{2}$$

$$\sum_{\forall l \in \Omega^{\text{line}}} x_l^{\text{line}} \le N^{\text{line}} \tag{3}$$

$$\sum_{\forall k \in \Omega^{\text{link}}} x_k^{\text{link}} \le N^{\text{link}} \tag{4}$$

where Ω_l^{bus} is the set of two end nodes of line l; Ω^{line} is the set of all distribution lines; Ω^{bus} is the set of all distribution nodes; Ω^{com} is the set of communication links; s_i^{rcs} is a 0–1 variable indicating whether there is an RCS on the side of node i of line l ($s_{i,l}^{\text{rcs}} = 1$ if yes); m_i^{dg} is a 0–1 variable indicating whether there is a DG at node i ($m_i^{\text{dg}} = 1$ if yes); x_l^{line} is a 0–1 variable indicating whether distribution line l is hardened ($x_l^{\text{line}} = 1$ if yes); x_k^{link} is a 0–1 variable indicating whether the communication link k is hardened ($x_k^{\text{link}} = 1$ if yes); and N^{rcs} and N^{dg} indicate the limited number of RCSs and DGs, respectively. N^{line} and N^{link} are the upper limits of the reinforced distribution lines and the reinforced communication link, respectively.

3.2. Prevention Stage Constraints

In the prevention stage, only the distribution lines equipped with RCSs can participate in the fast network reconfiguration, as shown in Equation (5). Equation (6) indicates that a distribution line is closed only if both ends of the line are closed. Since Equation (6) is a nonlinear constraint, it can be transformed into a linearized form, as shown in Equation (7). Equations (8)–(10) show the radial network topology constraints for the distribution network based on the idea of single commodity flow [19].

$$z_{i,l}^{\text{org}} - s_{i,l}^{\text{rcs}} \le z_{i,l}^{\text{pre}} \le z_{i,l}^{\text{org}} + s_{i,l}^{\text{rcs}}, \forall i \in \Omega_l^{\text{bus}}, \forall l \in \Omega^{\text{line}} \tag{5}$$

$$z_l^{\text{pre}} = z_{i,l}^{\text{pre}} z_{j,l}^{\text{pre}}, \forall i, j \in \Omega_l^{\text{bus}}, i \ne j, \forall l \in \Omega^{\text{line}} \tag{6}$$

$$\begin{cases} z_l^{\text{pre}} \le z_{i,l}^{\text{pre}} \\ z_l^{\text{pre}} \le z_{j,l}^{\text{pre}} \\ z_l^{\text{pre}} \ge z_{i,l}^{\text{pre}} + z_{j,l}^{\text{pre}} - 1 \end{cases}, \forall i, j \in \Omega_l^{\text{bus}}, i \ne j, \forall l \in \Omega^{\text{line}} \tag{7}$$

$$1 - M\gamma_i^{\text{pre}} \le \sum_{l \in \Omega_i^{\text{line}}} F_l^{\text{pre}} \le 1 + M\gamma_i^{\text{pre}}, \forall i \in \Omega^{\text{bus}} \tag{8}$$

$$-Mz_l^{\text{pre}} \le F_l^{\text{pre}} \le Mz_l^{\text{pre}}, l \in \Omega^{\text{line}} \tag{9}$$

$$\sum_{l \in \Omega^{\text{line}}} z_l^{\text{pre}} = N^{\text{bus}} - \sum_{i \in \Omega^{\text{bus}}} \gamma_i \tag{10}$$

where Ω_i^{line} is the set of lines connected to node i; $z_{i,l}^{\text{org}}$ and $z_{i,l}^{\text{pre}}$ are 0–1 variables indicating whether the end i of line l is closed in the initial stage and the prevention stage, respectively ($z_{i,l}^{\text{org}} = 1/z_{i,l}^{\text{pre}} = 1$ if yes); z_l^{pre} is a 0–1 variable indicating whether line l is closed in the prevention stage ($z_l^{\text{pre}} = 1$ if yes); M is a large number; γ_i^{pre} is a 0–1 variable indicating whether node i is a root node in the prevention stage ($\gamma_i^{\text{pre}} = 1$ if yes); F_l^{pre} is the fictitious

commodity flow flowing through line l in the prevention stage; and N^{bus} is the total number of nodes.

The power flow and safety constraints in the prevention stage are shown as Equations (11)–(18). Equations (11) and (12) are the active and reactive power injection balance constraints for node i. Equation (13) is the linearized Distflow constraint [20]. Equations (14) and (15) are the capacity limits of the distribution lines. Equation (16) shows the voltage limits. Equations (17) and (18) denote the constraints of the injected power of the DGs.

$$P_i^{\text{L}} - P_i^{\text{pre,D}} = \sum_{l \in \Omega_i^{\text{line}}} P_l^{\text{pre,F}}, \forall i \in \Omega^{\text{bus}} \tag{11}$$

$$Q_i^{\text{L}} - Q_i^{\text{pre,D}} = \sum_{l \in \Omega_i^{\text{line}}} Q_l^{\text{pre,F}}, \forall i \in \Omega^{\text{bus}} \tag{12}$$

$$M(1 - z_l^{\text{pre}}) \le V_i^{\text{pre}} - V_j^{\text{pre}} - (R_l P_l^{\text{pre,F}} + X_l Q_l^{\text{pre,F}})/U_0 \le -M(1 - z_l^{\text{pre}}), \forall i, j \in \Omega_l^{\text{bus}}, i \ne j, l \in \Omega^{\text{line}} \tag{13}$$

$$-z_l^{\text{pre}} P_l^{\text{F,max}} \le P_l^{\text{pre,F}} \le z_l^{\text{pre}} P_l^{\text{F,max}}, l \in \Omega^{\text{line}} \tag{14}$$

$$-z_l^{\text{pre}} Q_l^{\text{F,max}} \le Q_l^{\text{pre,F}} \le z_l^{\text{pre}} Q_l^{\text{F,max}}, l \in \Omega^{\text{line}} \tag{15}$$

$$V_i^{\min} \le V_i^{\text{pre}} \le V_i^{\max}, \forall i \in \Omega^{\text{bus}} \tag{16}$$

$$0 \le P_i^{\text{pre,D}} \le m_i^{\text{dg}} P_i^{\text{D,max}}, \forall i \in \Omega^{\text{bus}} \tag{17}$$

$$0 \le Q_i^{\text{pre,D}} \le m_i^{\text{dg}} Q_i^{\text{D,max}}, \forall i \in \Omega^{\text{bus}} \tag{18}$$

where P_i^{L} and Q_i^{L} are the active and reactive load demands at node i; $P_i^{\text{pre,D}}$ and $Q_i^{\text{pre,D}}$ are the active and reactive outputs of the DG in the prevention stage; $P_l^{\text{pre,F}}$ and $Q_l^{\text{pre,F}}$ are the active and reactive power flow of line l in the prevention stage; V_i^{pre} is the voltage at node i in the prevention stage; R_l and X_l are the resistance and reactance of line l, respectively; U_0 is the reference voltage; $P_l^{\text{F,max}}$ and $Q_l^{\text{F,max}}$ are the upper limit of the active and reactive capacity of the line; $V_i^{\max}$ and $V_i^{\min}$ are the upper and lower limits of the voltage at node i; and $P_i^{\text{D,max}}$ and $Q_i^{\text{D.max}}$ are the upper limit of the active and reactive output of the DG at node i.

3.3. Degradation Stage Constraints

In the degradation stage, based on the idea of fault propagation [21], each node in the system can be analyzed in detail whether it is affected by the fault so as to determine whether the node is involved in the faulted area or not. For $\forall c \in \Omega^{\text{sce}}$ (Ω^{sce} is the set of fault scenarios), the fault propagation constraints are shown as Equations (19)–(21). Constraint (19) indicates that line l will not be damaged until it is unreinforced and under attack. Equation (20) indicates that if there is a fault on line l, the closed end of i will be involved in the faulted area. Equation (21) indicates that the nodes at the two ends of a closed line will be involved in the same faulted area or the same non-faulted area.

$$f_{l,c} = u_{l,c}(1 - x_l^{\text{line}}), \forall l \in \Omega^{\text{line}}, \forall c \in \Omega^{\text{sce}} \tag{19}$$

$$\mu_{i,c}^{\text{deg}} \ge f_{l,c} z_{i,l}^{\text{pre}}, \forall i \in \Omega_l^{\text{line}}, \forall l \in \Omega^{\text{line}} \tag{20}$$

$$\begin{cases} \mu_{i,c}^{\text{deg}} + z_l^{\text{pre}} - 1 \le \mu_{j,c}^{\text{deg}} \\ \mu_{j,c}^{\text{deg}} + z_l^{\text{pre}} - 1 \le \mu_{i,c}^{\text{deg}} \end{cases}, \forall i, j \in \Omega_i^{\text{line}}, i \ne j, \forall l \in \Omega^{\text{line}} \tag{21}$$

where $u_{l,c}$ is a 0–1 variable indicating whether line l is under physical attack under scenario c ($u_{l,c} = 1$ if yes); $f_{l,c}$ is a 0–1 variable indicating whether line l is faulted under scenario c

($f_{l,c} = 1$ if yes); and $\mu_{i,c}^{\text{deg}}$ is a 0–1 variable for indicating node i is involved in the faulted area under scenario c during the degradation stage ($\mu_{i,c}^{\text{deg}} = 1$ if yes).

The impact of information attacks on the communication network is regarded as data packet loss. The communication link with data packet loss is disconnected, but the communication link with hardening measures can still work normally. As shown in Equation (22), for communication links that have undergone reinforcement measures, they can still maintain normal operation even under cyber-attacks.

$$a_{k,c} = 1 - w_{k,c}(1 - x_k^{\text{link}}), \forall k \in \Omega^{\text{link}}, \forall c \in \Omega^{\text{sce}} \tag{22}$$

where $w_{k,c}$ is a 0–1 variable indicating whether the communication link k is under a cyber-attack under scenario c ($w_{k,c} = 1$ if yes) and $a_{k,c}$ is a 0–1 variable indicating whether the communication link k is faulted under scenario c ($a_{k,c} = 0$ if yes).

The key to ensuring the normal operation of a communication network lies in maintaining effective connections between communication nodes and the operational center. To accurately determine whether the communication nodes are connected to the operational center, a virtual flow network with the same topology as the communication network has been constructed, where the communication links are different from the distribution network, and the communication nodes are corresponding to the distribution network nodes, as shown in Equations (23)–(27). In Equation (23), the operational center acts as a virtual source in the virtual network, responsible for providing the injection of virtual flow. Equation (24) represents the balance constraint of the virtual flow. Equation (25) indicates that only closed communication links can have virtual flow passing through them. Equation (26) states that if a node is a source node, it has a unit virtual load, meaning that the operational center always maintains effective communication with it. Equation (27) states that if a communication link is closed and one end of the node is communicating normally, then the other end of the node also belongs to the normal communication area.

$$0 \le G_{i,c}^{\text{com}} \le M g_i^{\text{com}}, \forall i \in \Omega^{\text{node}} \tag{23}$$

$$G_{i,c}^{\text{com}} - \tau_{i,c} = \sum_{k \in \Omega_i^{\text{link}}} F_{k,c}^{\text{com}}, \forall k \in \Omega^{\text{link}}, \forall i \in \Omega_k^{\text{node}} \tag{24}$$

$$-M a_{k,c} \le F_{k,c}^{\text{com}} \le M a_{k,c}, \forall k \in \Omega^{\text{link}} \tag{25}$$

$$\tau_{i,c} \ge g_{i,c}^{\text{com}}, \forall i \in \Omega^{\text{node}} \tag{26}$$

$$\begin{cases} \tau_{i,c} + a_{k,c} - 1 \le \tau_{j,c} \\ \tau_{j,c} + a_{k,c} - 1 \le \tau_{i,c} \end{cases}, \forall i, j \in \Omega_k^{\text{node}}, \forall k \in \Omega^{\text{link}} \tag{27}$$

where Ω^{node} is the set of all communication nodes; Ω_k^{node} is the set of two end-nodes of communication link k; $G_{i,c}^{\text{com}}$ is the injected virtual flow; g_i^{com} is a 0–1 variable indicating whether node i is a source node ($g_i^{\text{com}} = 1$ if yes); F_k^{in} is the virtual flow in communication link k; and $\tau_{i,c}$ is a 0–1 variable indicating whether node i is connected to the operational center ($\tau_{i,c} = 1$ if yes).

Due to distribution line faults, the load supply within the faulted area cannot be met, as shown in Equations (28) and (29). Affected by communication link faults, to ensure the safety of the distribution network, once a communication node fails, the load connected to that node must be immediately curtailed, as described in Equations (30) and (31).

$$\mu_{i,c}^{\text{deg}} P_i^{\text{L}} \le P_{i,c}^{\text{deg,C}} \le P_i^{\text{L}}, \forall i \in \Omega^{\text{bus}} \tag{28}$$

$$\mu_{i,c}^{\text{deg}} Q_i^{\text{L}} \le Q_{i,c}^{\text{deg,C}} \le Q_i^{\text{L}}, \forall i \in \Omega^{\text{bus}} \tag{29}$$

$$(1-\tau_{i,c})P_i^{\mathrm{L}} \le P_{i,c}^{\mathrm{deg,C}} \le P_i^{\mathrm{L}}, \forall i \in \Omega^{\mathrm{node}} \tag{30}$$

$$(1-\tau_{i,c})Q_i^{\mathrm{L}} \le Q_{i,c}^{\mathrm{deg,C}} \le Q_i^{\mathrm{L}}, \forall i \in \Omega^{\mathrm{node}} \tag{31}$$

where $P_{i,c}^{\mathrm{deg,C}}$ and $Q_{i,c}^{\mathrm{deg,C}}$ are the loss of the active and reactive load of node i under the degradation stage under scenario c. It should be noted that communication nodes coincide with distribution network nodes in this paper, i.e., $\Omega^{\mathrm{bus}} = \Omega^{\mathrm{node}}$.

3.4. Recovery Stage Constraints

The network topology constraints in the recovery stage are shown in Equations (32)–(37). Equation (32) indicates that during the recovery stage, adjustments to the line status can only be made when the line equipped with RCS maintains normal communication. Equation (33) shows that the state of the line depends on whether the switches at its ends are closed or not and the line itself is faulted or not, with the linearization constraints shown in Equation (34). Equations (35)–(37) are the radial network topology constraints.

$$z_{i,l}^{\mathrm{pre}} - s_{i,l}^{\mathrm{rcs}}\tau_{i,c} \le z_{i,l.c}^{\mathrm{ir}} \le z_{i,l}^{\mathrm{pre}} + s_{i,l}^{\mathrm{rcs}}\tau_{i,c}, \forall i \in \Omega_l^{\mathrm{bus}}, \forall l \in \Omega^{\mathrm{line}} \tag{32}$$

$$z_{l,c}^{\mathrm{ir}} = z_{i,l,c}^{\mathrm{ir}} z_{j,l,c}^{\mathrm{ir}}(1-f_{l,c}), \forall i,j \in \Omega_l^{\mathrm{bus}}, i \ne j, \forall l \in \Omega^{\mathrm{line}} \tag{33}$$

$$\begin{cases} z_{l,c}^{\mathrm{ir}} \le z_{i,l.c}^{\mathrm{ir}} \\ z_{l,c}^{\mathrm{ir}} \le z_{j,l,c}^{\mathrm{ir}} \\ z_{l,c}^{\mathrm{ir}} \le (1-f_{l,c}) \\ z_{l,c}^{\mathrm{ir}} \ge z_{i,l.c}^{\mathrm{ir}} + z_{j,l,c}^{\mathrm{ir}} - f_{l,c} - 1 \end{cases}, \forall i,j \in \Omega_l^{\mathrm{bus}}, i \ne j, \forall l \in \Omega^{\mathrm{line}} \tag{34}$$

$$1 - M\gamma_{i,c}^{\mathrm{ir}} \le \sum_{l \in \Omega_i^{\mathrm{line}}} F_{l,c}^{\mathrm{ir}} \le 1 + M\gamma_{i,c}^{\mathrm{ir}}, \forall i \in \Omega^{\mathrm{bus}} \tag{35}$$

$$-Mz_{l,c}^{\mathrm{ir}} \le F_{l,c}^{\mathrm{ir}} \le Mz_{l,c}^{\mathrm{ir}}, l \in \Omega^{\mathrm{line}} \tag{36}$$

$$\sum_{l \in \Omega^{\mathrm{line}}} z_{l,c}^{\mathrm{ir}} = N^{\mathrm{bus}} - \sum_{i \in \Omega^{\mathrm{bus}}} \gamma_{i,c}^{\mathrm{ir}} \tag{37}$$

where $z_{i,l,c}^{\mathrm{ir}}$ and $z_{l,c}^{\mathrm{ir}}$ are 0–1 variables indicating whether the end i of line l and line l are closed under scenario c during the recovery stage, respectively ($z_{i,l,c}^{\mathrm{ir}} = 1/z_{l,c}^{\mathrm{ir}} = 1$ if yes); $\gamma_{i,c}^{\mathrm{ir}}$ is a 0–1 variable indicating whether node i under scenario c is the root node during the recovery stage ($\gamma_{i,c}^{\mathrm{ir}} = 1$ if yes); and $F_{l,c}^{\mathrm{ir}}$ is the commodity flow of line l under scenario c during the recovery stage.

Similar to the degradation stage, it is also necessary to determine whether a node is in a faulted area or not in the recovery stage, as shown in Equations (38) and (39).

$$\mu_{i,c}^{\mathrm{ir}} \ge f_{l,c} z_{i,l.c}^{\mathrm{ir}}, \forall i \in \Omega_l^{\mathrm{bus}}, \forall l \in \Omega^{\mathrm{line}} \tag{38}$$

$$\begin{cases} \mu_{i,c}^{\mathrm{ir}} + z_{l,c}^{\mathrm{ir}} - 1 \le \mu_{j,c}^{\mathrm{ir}} \\ \mu_{j,c}^{\mathrm{ir}} + z_{l,c}^{\mathrm{ir}} - 1 \le \mu_{i,c}^{\mathrm{ir}} \end{cases}, \forall i,j \in \Omega_l^{\mathrm{bus}}, i \ne j, \forall l \in \Omega^{\mathrm{line}} \tag{39}$$

where $\mu_{i,c}^{\mathrm{ir}}$ is a 0–1 variable indicating whether node i under scenario c belongs to the faulted area.

For $\forall c \in \Omega^{\mathrm{sce}}$, the power flow and safety constraints in the recovery stage are shown in Equations (40)–(51). Different from the prevention stage, the loss of load is considered in Equations (40) and (41); the load supply cannot be satisfied, and the DG will be out of

service within the faulted area, as shown in Equations (46)–(51). The remaining variables and constraints are similar in meaning to the prevention stage and will not be repeated here.

$$P_i^{\mathrm{L}} - P_{i,c}^{\mathrm{ir,D}} - P_{i,c}^{\mathrm{ir,C}} = \sum_{l \in \Omega_i^{\mathrm{line}}} P_{l,c}^{\mathrm{ir,F}}, \forall i \in \Omega^{\mathrm{bus}} \tag{40}$$

$$Q_i^{\mathrm{L}} - Q_{i,c}^{\mathrm{ir,D}} - Q_{i,c}^{\mathrm{ir,C}} = \sum_{l \in \Omega_i^{\mathrm{line}}} Q_{l,c}^{\mathrm{ir,F}}, \forall i \in \Omega^{\mathrm{bus}} \tag{41}$$

$$-M(1 - z_{l,c}^{\mathrm{ir}}) \le V_{i,c}^{\mathrm{ir}} - V_{j,c}^{\mathrm{ir}} - (R_l P_{l,c}^{\mathrm{ir,F}} + X_l Q_{l,c}^{\mathrm{ir,F}})/U_0 \le M(1 - z_{l,c}^{\mathrm{ir}}), \forall i, j \in \Omega_l^{\mathrm{bus}}, i \ne j, l \in \Omega^{\mathrm{line}} \tag{42}$$

$$-z_{l,c}^{\mathrm{ir}} P_l^{\mathrm{F,max}} \le P_{l,c}^{\mathrm{ir,F}} \le z_{l,c}^{\mathrm{ir}} P_l^{\mathrm{F,max}}, l \in \Omega^{\mathrm{line}} \tag{43}$$

$$-z_{l,c}^{\mathrm{ir}} Q_l^{\mathrm{F,max}} \le Q_{l,c}^{\mathrm{ir,F}} \le z_{l,c}^{\mathrm{ir}} Q_l^{\mathrm{F,max}}, l \in \Omega^{\mathrm{line}} \tag{44}$$

$$V_i^{\min} \le V_{i,c}^{\mathrm{ir}} \le V_i^{\max}, \forall i \in \Omega^{\mathrm{bus}} \tag{45}$$

$$0 \le P_{i,c}^{\mathrm{ir,D}} \le \tau_{i,c}(1 - \mu_{i,c}^{\mathrm{ir}}) m_i^{\mathrm{dg}} P_i^{\mathrm{D,max}}, \forall i \in \Omega^{\mathrm{bus}} \tag{46}$$

$$0 \le Q_{i,c}^{\mathrm{ir,D}} \le \tau_{i,c}(1 - \mu_{i,c}^{\mathrm{ir}}) m_i^{\mathrm{dg}} Q_i^{\mathrm{D,max}}, \forall i \in \Omega^{\mathrm{bus}} \tag{47}$$

$$(1 - \tau_{i,c}) P_i^{\mathrm{L}} \le P_{i,c}^{\mathrm{ir,C}} \le P_i^{\mathrm{L}}, \forall i \in \Omega^{\mathrm{bus}} \tag{48}$$

$$(1 - \tau_{i,c}) Q_i^{\mathrm{L}} \le Q_{i,c}^{\mathrm{ir,C}} \le Q_i^{\mathrm{L}}, \forall i \in \Omega^{\mathrm{bus}} \tag{49}$$

$$\mu_{i,c}^{\mathrm{ir}} P_i^{\mathrm{L}} \le P_{i,c}^{\mathrm{ir,C}} \le P_i^{\mathrm{L}}, \forall i \in \Omega^{\mathrm{bus}} \tag{50}$$

$$\mu_{i,c}^{\mathrm{ir}} Q_i^{\mathrm{L}} \le Q_{i,c}^{\mathrm{ir,C}} \le Q_i^{\mathrm{L}}, \forall i \in \Omega^{\mathrm{bus}} \tag{51}$$

3.5. Objective Function

To minimize the total expected loss of load during the degradation stage and recovery stage, the objective function is shown as Equation (52).

$$\min C = \sum_{\forall c \in \Omega^{\mathrm{snr}}} \left(T^{\mathrm{deg}} \sum_{i \in \Omega^{\mathrm{bus}}} \omega_i P_{i,c}^{\mathrm{deg,C}} + T^{\mathrm{ir}} \sum_{i \in \Omega^{\mathrm{bus}}} \omega_i P_{i,c}^{\mathrm{ir,C}} \right) \tag{52}$$

where C indicates the total expected loss of load; p_c is the probability of scenario c; T^{deg} and T^{ir} are the duration of the degradation stage and the recovery stage; and ω_i is the load weight.

For a clearer representation of the system's resilience level, the following indicator is used. This indicator specifically reflects the percentage of load for which the system can maintain normal power supply during the degradation stage and the post-event recovery stage.

$$R = \left(1 - \frac{C}{(T^{\mathrm{deg}} + T^{\mathrm{ir}}) \sum_{i \in \Omega^{\mathrm{bus}}} \omega_i P_i^{\mathrm{L}}} \right) \times 100\% \tag{53}$$

4. Case Study

4.1. Parameter Setting

In this section, the IEEE 33-node system and its corresponding communication network are employed to validate the effectiveness of the proposed method. The system comprises 33 nodes and 37 lines, among which lines L33 to L37 are tie lines with a capacity of 5 MVA each, and the total load is 3.715 MW + j2.300 MVar. The voltage limits at each node are set in the range of [0.95, 1.05] p.u. Nodes 4, 12, 16, 25, and 30 are designated as critical

load nodes with a weight of 3, while the remaining nodes have a weight of 1 for non-critical loads. Centralized communication is mainly considered, and the communication network consists of one operational center, 37 communication links, and 33 communication nodes corresponding to the distribution network nodes, with the communication links detailed in Table 1. Five different fault scenarios are randomly generated to consider the above uncertainties, each containing five faulted distribution lines and two faulted communication links, with each scenario having a probability of occurrence $p_c = 1/5$, as shown in Table 2. The upper limits for the number of RCSs and DGs are set at 10 and 4, respectively. The capacity of the controllable DG is set at 0.4 MVA [22]. The upper limits for the number of reinforced lines and communication links are set at 4 and 3, respectively. The values of $T^{\deg}$ and T^{ir} are set at 0.5 h each [23]. The case study is implemented using Matlab, and the Gurobi optimizer is invoked through the Yalmip toolbox for optimization solutions.

Table 1. Topology of the communication network.

Line Number	Start Node	End Node	Line Number	Start Node	End Node	Line Number	Start Node	End Node
1	6	1	14	15	3	27	6	28
2	6	5	15	6	12	28	28	30
3	5	1	16	12	20	29	28	17
4	1	19	17	20	7	30	28	8
5	1	27	18	12	13	31	8	2
6	1	26	19	13	4	32	28	31
7	1	32	20	13	16	33	31	29
8	32	22	21	13	18	34	6	21
9	6	24	22	13	10	35	15	12
10	24	33	23	13	11	36	28	12
11	26	27	24	13	23	37	20	13
12	6	14	25	23	9			
13	14	15	26	13	25			

Table 2. Fault scenarios.

Scenario Number	Faulted Lines	Faulted Communication Links
1	L4, L7, L14, L23, L28	L8, L19
2	L8, L10, L17, L24, L32	L4, L21
3	L2, L11, L19, L26, L31	L14, L24
4	L5, L13, L16, L18, L29	L17, L32
5	L3, L9, L12, L22, L26	L4, L23

4.2. Analysis of Basic Results

The results of the resource optimization allocation in the planning and prevention stages are analyzed in Figures 3 and 4. In the stage of resource allocation, reinforcement measures are carried out for distribution lines L24, L29, L31, and L32 to ensure the stable operation of the distribution network. DGs are deployed at nodes 24, 25, 30, and 33 to provide load support. Meanwhile, communication links L4, L8, and L32 are hardened against network cyber-attacks. Network pre-reconfiguration based on RCSs in the prevention stage. The distribution network is divided into two zones, in each of which at least one substation or DG exists to supply it. During the prevention stage, the distribution network is pre-reconfigured into two zones using an RCS, with at least one substation or DG providing power to each zone.

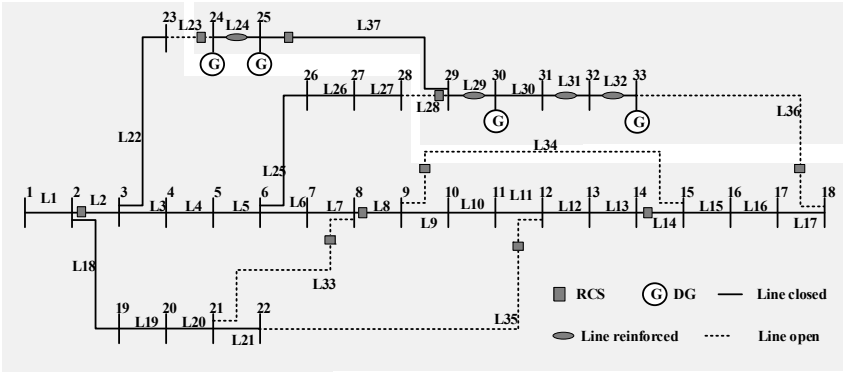


Figure 3. Results of distribution line reinforcement, resource allocation, and network pre-configuration.

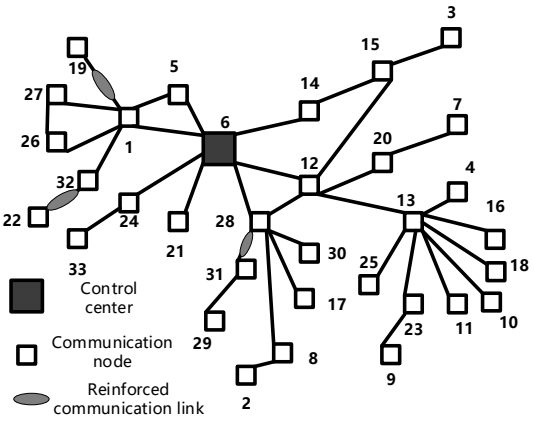
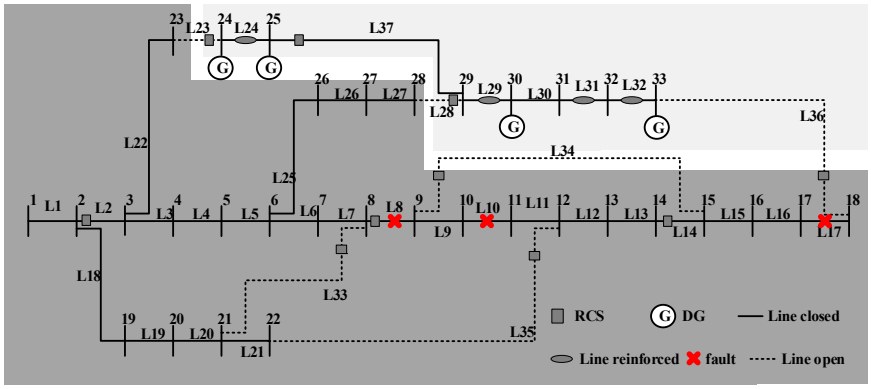
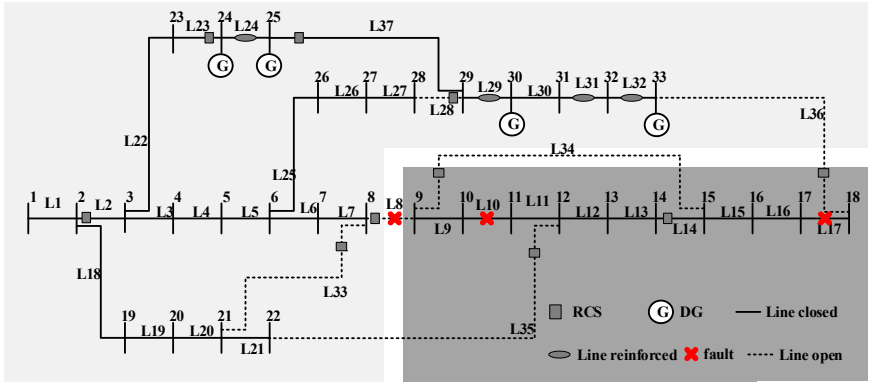


Figure 4. Results of communication link reinforcement. (Topology of the communication network has been listed in Table 1).

Figure 5 shows the analysis of the operation results of the multi-stage post-accident recovery process in scenario 2. The process of the degradation stage (fault propagation and affected area identification) and recovery stage (fault isolation and power restoration) of the system under extreme events is shown. Where, light gray represents the non-fault area with power supply, and gray represents the fault area affected by the fault. During the degradation stage, it can be observed that the distribution lines L24 and L32, due to prior reinforcement measures, successfully prevented faults from occurring when encountering the extreme event. Similarly, the communication link L4, which also underwent reinforcement, prevented information loss in the communication network during a cyber-attack. At the same time, preventive islanding is formed through pre-reconfiguration using RCSs, allowing some areas to maintain normal operation independently of the faults (such as nodes 24–25 and 29–33, which include key nodes 25 and 30). During the recovery stage, network reconfiguration using RCSs was utilized to further restore system load (such as nodes 1–7, 19–33).



(**a**) Degeneration stage



(**b**) Recovery stage

Figure 5. Topology of the distribution network after the extreme event. (**a**): Topology of the distribution network in the degeneration stage; (**b**): Topology of the distribution network in the degeneration stage.

4.3. Analysis of the Effects of Considering Cyber–Physical Attacks and Collaborative Reinforcement Measures

To validate the effects of cyber–physical attacks, three cases are set for analysis, as shown in Table 3.

Table 3. Description of different attack cases.

Case	Case Description
Case 1	Only physical attacks on the distribution network are considered.
Case 2	Only cyber-attacks on the communication network are considered.
Case 3	Cyber–physical attacks are both considered.

Under the conditions where the upper limit of the DGs is 4 and the upper limits of the reinforced distribution lines and communication links are 4 and 0, respectively, the percentage of load loss under different attack scenarios and RCS allocation schemes is shown in Figure 6. In Cases 1 and 3, as the number of RCSs increases, the percentage of load loss exhibits a decreasing trend. However, compared to Case 1, the reduction in load loss percentage is significantly smaller in Case 3 when maintaining the same RCS allocation scheme, indicating that cyber–physical coordinated attacks constrain the effectiveness of RCS allocation in enhancing system resilience. In Case 2, the load loss percentage remains almost constant, primarily because the RCS allocation scheme is ineffective against cyber-attacks and cannot effectively mitigate their impact.

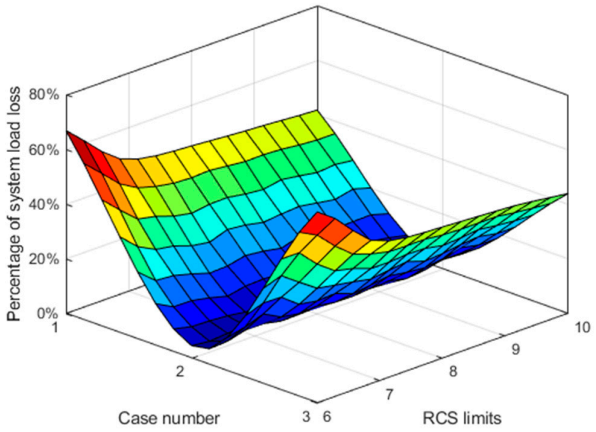


Figure 6. Percentage of system load loss for different attack scenarios and different RCS allocation schemes.

Under the conditions where the upper limit of the RCS quantity is 10 and the upper limits of reinforced distribution lines and communication links are 4 and 0, respectively, the results of system load loss percentage under different attack scenarios and DG allocation schemes are shown in Figure 7. In Cases 1 and 3, as the number of DGs increases, the system load loss percentage also shows a decreasing trend. Nevertheless, compared to Case 1, the reduction in system load loss percentage is notably smaller in Case 3 when maintaining the same DG allocation scheme, suggesting that cyber–physical coordinated attacks also restrict the effectiveness of DG allocation in enhancing system resilience. Furthermore, compared to Cases 1 and 2, the load loss percentage in Case 3 is significantly higher, demonstrating that compared to single attack strategies, cyber–physical coordinated attacks have a more intense impact on the distribution network, resulting in greater load losses and exacerbating the vulnerability and instability of the distribution network.

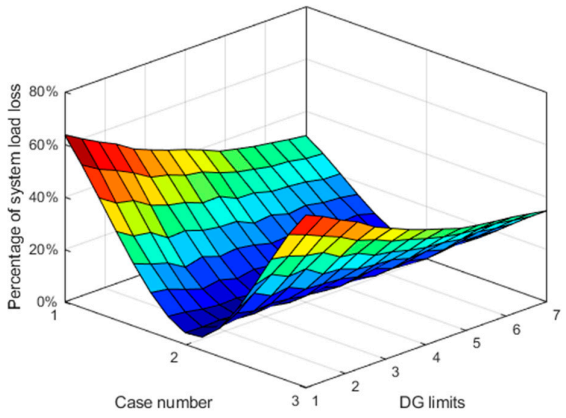


Figure 7. Percentage of system load loss for different attack scenarios and different DG allocation schemes.

Furthermore, to validate the effectiveness of considering communication link reinforcement collaboratively, a comparative analysis is conducted between two cases: one with and one without communication link reinforcement. The number of cyber-attacks is set to be two and three, respectively, while the number of physical attacks is set to be five. In terms of resource allocation, the number of reinforced communication links is set to be 3, the number of reinforced distribution lines is set to be 4, and the number of RCSs and DGs is set to be 10 and 4, respectively. Based on these, a comparative analysis of the two cases is conducted, with results presented in Table 4.

Table 4. Optimized resource allocation before and after communication link reinforcement strategy.

Number of Cyber Attacks	Whether Communication Network Reinforcement is Considered	Location of RCSs		Location of DGs	Communications Link Reinforcement Locations	Resilience Level
		The Beginning End of the Line	The Terminal End of the Line			
2	yes	L2, L8, L14, L33–L37	L23, L28	24, 25, 30, 33	L4, L8, L32	58.19%
	No	L5, L8, L33–L37	L2, L23, L28	24, 25, 32, 33	not have	54.59%
3	yes	L8, L24, L33–L37	L10, L14, L28	18, 25, 29, 30	L24, L32, L36	57.08%
	No	L8, L33–L37	L10, L14, L24, L28	10, 25, 30, 32	not have	52.84%

When the number of cyber-attacks is two, the resilience level of the reinforced distribution network is improved by 3.6% compared to the case without communication link reinforcement. When the number of cyber-attacks is three, the resilience level of the reinforced distribution network is improved by 4.24% compared to the scenario without communication link reinforcement. This indicates that reinforcing communication links can enhance the distribution network's ability to withstand cyber–physical synergistic attacks.

Additionally, there are significant changes in the locations of RCSs and DGs between the two cases. After the communication link is strengthened, more communication nodes can survive the attack, providing more node options for the isolation and recovery stage of the RCSs and DGs. This increases the flexibility of resource allocation, allowing the system to adjust resource allocation based on real-time conditions to maximize recovery.

4.4. Analysis of the Effects of Considering Collaborative Resource Allocation

In this section, three additional cases are introduced to validate the effectiveness of the method proposed in this paper. The descriptions of the cases are shown in Table 5. The load recovery curves for the four cases based on the scenario set in Table 2 are shown in Figure 8.

Table 5. Description of different cases.

Case	Case Description
Case 1	The methodology proposed in this paper
Case 2	Fixed DG position [14]
Case 3	Network pre-configuration is not performed in the prevention stage [24]
Case 4	Line reinforcement allocation is not performed

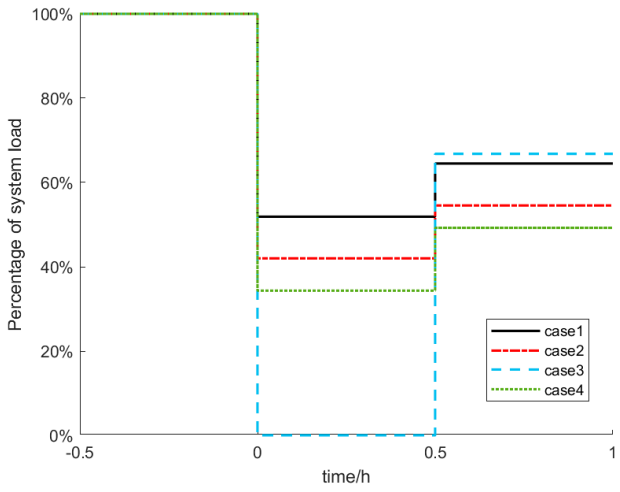


Figure 8. Load curves for different cases.

In the aforementioned scenario, the resilience level of the system is calculated as R = 58.19% using (53), with the resilience level for each individual scenario presented in Table 6. By coordinating a series of strategies, including the configuration of distributed generations (DGs), remote-controlled switches (RCSs), and the reinforcement of distribution lines and communication links, the system's emergency response capability and recovery speed can be significantly enhanced.

Table 6. The level of system resilience in each scenario.

Scenario	Resilience level
Scenario 1	60.95%
Scenario 2	67.525%
Scenario 3	53.125%
Scenario 4	51.89%
Scenario 5	54.71%

In Case 2, the system's resilience level was 48.265%. The DGs were fixed at nodes 4, 11, 18, and 23, which failed to optimize their deployment positions. Consequently, the synergistic effect between DGs and RCSs was not fully utilized, hindering the effective isolation of fault areas and the formation of restorative islands. As a result, the system incurred relatively large load losses during the degradation and recovery stages due to the suboptimal DG configuration. By optimizing the DG placement, the flexibility in positioning DGs within the distribution network can be markedly improved, enabling them to be more accurately deployed in crucial locations based on actual needs. This approach not only minimizes load losses but also reduces the risk of electricity consumption disruptions for power users, thereby significantly boosting the resilience of the distribution network.

In Case 3, the system's resilience level was 33.395%. Since the distribution network was not pre-reconfigured during the prevention stage, it remained highly interconnected. Such a tightly coupled network structure meant that any line failure could trigger widespread power outages across the distribution network. Therefore, pre-reconfiguring the distribution network is of paramount importance. By doing so, the network structure can be optimized to decrease the degree of interconnectivity, effectively preventing the rapid propagation of faults. This measure notably enhances the resilience level of the distribution network and reduces the scope of power outages during the degradation stage.

In Case 4, the system's resilience level was 41.785%. The lack of consideration for implementing reinforcement measures on distribution network lines rendered the network particularly susceptible to upcoming extreme events. The inadequate response and defense capabilities led to a substantial increase in fault areas within the distribution network during extreme events. Consequently, to ensure the normal power demands of users and improve the response and resilience of the distribution network, it is imperative to prioritize the reinforcement of the distribution network lines. Through scientific and reasonable reinforcement design, the resilience and reliability of the distribution network lines can be significantly enhanced.

5. Conclusions

To enhance the resilience of distribution networks against cyber–physical coordinated attacks, this paper proposes an optimal resource allocation method for distribution networks that considers the coupling between power and communication networks. Through the IEEE 33-node system case study, it is demonstrated that the proposed method can effectively leverage RCSs and DGs to form preventive islands during the prevention stage. In the degradation stage, the distribution network identifies faulted and non-faulted areas based on the fault propagation model, while the communication network assesses the fault

status of communication nodes using the virtual flow model. During the recovery stage, RCSs with normal communication are utilized for rapid fault isolation, and in conjunction with DGs with normal communication, restorative islands are formed. This approach achieves effective RCS and DG allocation, as well as power line and communication link reinforcement, thereby enhancing the resilience level of the distribution network.

In future work, the impact of communication delays and decentralized communication architecture will be fully considered. Communication delays may prevent the rapid transmission of fault information to the operational center, thus interfering with the accurate determination and timely isolation of the fault area, which may lead to a long duration time of the degradation stage. It can also cause the recovery stage remote-control command to fail to reach the target device in time, thus increasing the response time of the switching operation. In a decentralized communication architecture, the communication network is divided into multiple layers, each of which is responsible for different communication tasks and data flows. This structure has high flexibility and scalability, so each level should be managed and optimized relatively independently, showing different characteristics with centralized communication. Therefore, based on the existing research, the effects of communication delay and decentralized communication structure will be further explored in the future.

Author Contributions: Conceptualization, J.L. and C.Q.; methodology, J.L. and C.Q.; validation, K.S. and X.C.; formal analysis, K.S. and X.C.; writing—original draft preparation, K.S. and X.C.; writing—review and editing, J.L.; visualization, K.S.; supervision, C.Q. All authors have read and agreed to the published version of the manuscript.

Funding: This research received no external funding.

Data Availability Statement: The data is unavailable due to privacy or ethical restrictions.

Conflicts of Interest: The authors declare no conflicts of interest.

References

1. Liu, D.; Sheng, W.; Wang, Y.; Lu, Y.; Sun, C. Key Technologies and Trends of Cyber Physical System for Power Grid. *Proc. CSEE* **2015**, *35*, 3522–3531. [CrossRef]
2. Zhang, W.; Luo, H. Analysis of Distribution Network Resilience Improvement Strategy Considering Power-information-transportation Network Coupling. *Power Syst. Technol.* **2024**, *48*, 361–373. [CrossRef]
3. Guo, Q.; Xi, S.; Wang, J.; Sun, H. Comprehensive Security Assessment for a Cyber Physical Energy System: A Lesson from Ukraine's Blackout. *Autom. Electr. Power Syst.* **2016**, *40*, 145–147.
4. Rong, J.; Zhou, M.; Yuan, B.; Li, H.; Wu, Z. Resilience Assessment Method on Power Systems Under Typhoon Disaster Considering Failure Evolution Process. *Power Syst. Technol.* **2024**, *48*, 1114–1131. [CrossRef]
5. Liu, R.; Chen, C.; Liu, F.; Bie, Z. Power system resilience enhancement strategy considering cyber-physical interdependence under disasters: Development and prospects. *Electr. Mach. Control.* **2022**, *26*, 9–23. [CrossRef]
6. Rajaei, F.; Latify, M.; Ebrahimi, A. Incorporating DSO's Situational Awareness in Resilience-Oriented Distribution System Planning. *IEEE Trans. Smart Grid* **2023**, *14*, 1985–1997. [CrossRef]
7. Poudyal, A.; Shiva, P.; Anamika, D. Risk-based active distribution system planning for resilience against extreme weather events. *IEEE Trans. Sustain. Energy* **2022**, *14*, 1178–1192. [CrossRef]
8. Zhang, L.; Li, C. Optimal Anti-Icing and De-Icing Coordination Scheme for Resilience Enhancement in Distribution Networks Against Ice Storms. *IEEE Trans. Smart Grid* **2024**, *15*, 3486–3498. [CrossRef]
9. Wang, Y.; Li, K.; Xue, H.; Yu, A.; Mi, Y. Post-disaster Multi-source Cooperative Islanding Operation Strategy for Distribution Network Considering Mobile Energy Storage System Dispatching. *Autom. Electr. Power Syst.* **2024**, *48*, 62–72. [CrossRef]
10. Zhang, H.; Liu, C.; Zhao, Y.; Zhao, J.; Fu, Q. A Novel Proactive Operation Strategy to Enhance Power System Resilience. *Power Syst. Technol.* **2024**, *48*, 2012–2021. [CrossRef]
11. Liu, J.; Qin, C.; Yu, Y. A comprehensive resilience-oriented FLISR method for distribution systems. *IEEE Trans. Smart Grid* **2020**, *12*, 2136–2152. [CrossRef]
12. Liu, Z.; Wu, Q.; Shen, X. Post-Disaster Robust Restoration Scheme for Distribution Network Considering Rerouting Process of Cyber System With 5G. *IEEE Trans. Smart Grid* **2024**, *15*, 4478–4491. [CrossRef]

13. Xu, L.; Guo, Q.; Liu, X.; Sun, H. Robust Optimization Method of Communication Network to Improve Resilience of Cyber-Physical Power System. *Autom. Electr. Power Syst.* **2021**, *45*, 68–75. [CrossRef]
14. Ding, Z.; Zhang, Y.; Xie, S. Coordinated Defense Strategy for Cyber-physical System of Distribution Networks Considering Fault Cross-Domain Propagation and Network Coupling. *Power Syst. Technol.* **2024**, *48*, 5129–5137. [CrossRef]
15. Ye, Z.; Chen, C. Boost distribution system restoration with emergency communication vehicles considering cyber-physical interdependence. *IEEE Trans. Smart Grid* **2022**, *14*, 1262–1275. [CrossRef]
16. Ti, B. Resilience assessment and improvement for cyber-physical power systems under typhoon disasters. *IEEE Trans. Smart Grid* **2021**, *13*, 783–794. [CrossRef]
17. Liu, R.; Chen, C.; Ye, Z.; Bie, Z. Cooperative Cyber-physical Distribution System Restoration With UAV-based Emergency Communication UAV After Disasters. *Power Syst. Technol.* **2023**, *47*, 1218–1230. [CrossRef]
18. Zhang, H.; Chen, C. Resilient distribution system restoration with communication recovery by drone small cells. *IEEE Trans. Smart Grid* **2023**, *14*, 1325–1328. [CrossRef]
19. Ding, T.; Sun, K.; Huang, C. Mixed-integer linear program based splitting strategies for power system islanding operation considering network connectivity. *IEEE Syst. J.* **2018**, *12*, 350–359. [CrossRef]
20. Turitsyn, K.; Sulc, P.; Backhaus, S. Distributed control of reactive power flow in a radial distribution circuit with high photovoltaic penetration. In Proceedings of the IEEE PES General Meeting, Minneapolis, MN, USA, 25–29 July 2010; pp. 1–6. [CrossRef]
21. Ma, S.; Li, S.; Wang, Z. Resilience-oriented design of distribution systems. *IEEE Trans. Power Syst.* **2019**, *34*, 2880–2891. [CrossRef]
22. Liu, J.; Yu, Y.; Qin, C. Unified two-stage reconfiguration method for resilience enhancement of distribution systems. *IET Gener. Transm. Distrib.* **2019**, *13*, 1734–1745. [CrossRef]
23. Zeng, Y.; Qin, C.; Liu, J. Coordinating multiple resources for enhancing distribution system resilience against extreme weather events considering multi-stage coupling. *Int. J. Electr. Power Energy Syst.* **2022**, *138*, 107901. [CrossRef]
24. Sun, N.; Wu, G.; Chen, H. Resilience-Driven Hardening Strategies for Cyber-Physical Systems Considering Energy-Control Dependence. In Proceedings of the 2024 3rd International Conference on Energy and Electrical Power Systems (ICEEPS), Guangzhou, China, 14–16 July 2024; pp. 1253–1257. [CrossRef]

Disclaimer/Publisher's Note: The statements, opinions and data contained in all publications are solely those of the individual author(s) and contributor(s) and not of MDPI and/or the editor(s). MDPI and/or the editor(s) disclaim responsibility for any injury to people or property resulting from any ideas, methods, instructions or products referred to in the content.